Angewandte Chemie
Eine Zeitschrift der Gesellschaft Deutscher Chemiker

Supporting Information

High-Resolution NMR Determination of the Dynamic Structure of Membrane Proteins

*Mariusz Jaremko[+], Łukasz Jaremko[+], Saskia Villinger[+], Christian D. Schmidt[+], Christian Griesinger, Stefan Becker, and Markus Zweckstetter**

anie_201602639_sm_miscellaneous_information.pdf

SUPPORTING INFORMATION

MATERIALS AND METHODS

Sample preparation

The protein was expressed and purified according to previously published protocols[1,2]. For the current ^{15}N relaxation studies the E73V variant of human VDAC1 was prepared in U-^{2}H,^{15}N-labelled form and solubilized in 2% LDAO micelles. Perdeuteration was achieved by expressing in a minimal medium with 100% D_2O, perdeuterated unlabelled glucose and ^{15}N-ammonium chloride. The final E73V hVDAC1 concentration was 0.8 mM, pH 6.8, in 20 mM Bis-Tris, 7%/93% D_2O/H_2O.

NMR spectroscopy

The TROSY-based pulse sequence for measurement of ^{15}N-R_2 relaxation rates was adapted from the original $R_{1\rho}$ pulse program[3] where an appropriate CPMG block was introduced (**Supplementary Fig. 4**). The sequence was tested on ^{15}N-labelled ubiquitin and yielded within the experimental accuracy the same ^{15}N-R_2 rates as determined with HSQC-based schemes[4,5] (data not shown). ^{15}N-R_1 values were measured using the published TROSY-based pulse sequence[3] (**Supplementary Fig. 4**). ^{15}N-R_1 and ^{15}N-R_2 relaxation experiments were recorded on 600, 700 and 900 MHz Bruker Avance III spectrometers equipped with cryogenic probes. For all measurements the temperature was carefully adjusted to 37 °C using a standard sample of ethylene glycol. To achieve nearly complete signal recovery in between experiments, the recycle delay was set to 5 s. Further experimental parameters are shown in **Supplementary Table 4**.

Relaxation data analysis

Relaxation rates were obtained by 2-parameter non-linear mono-exponential fits of the obtained signal intensities over the applied relaxation delays using the MacDonald algorithm[6]. Errors were determined from the variance-covariance matrices. Only non-overlapping signals from the 2D ^{1}H-^{15}N TROSY experiments were selected for further analysis resulting in 179 R_1/R_2 pairs at each magnetic field (**Supplementary Fig. 5**). Average experimental errors of the measured relaxation rates are shown in **Supplementary Table 5**.

To subtract the high-frequency components of the spectral density functions, determination of $\rho=(2R_2'/R_1'-1)^{-1}$ would be required[7], where

$R_1' = R_1[1-1.249|\gamma_N/\gamma_H|(1-NOE)]$

$R_2' = R_2-1.079|\gamma_N/\gamma_H|R_1(1-NOE)$ [8]

NOE is the heteronuclear steady-state NOE, ρ contains information on the principal values of the diffusion tensor and on the orientation of the N-H vector with respect to the diffusion tensor frame[3,9]. The deviation of R_1' and R_2' from R_1 and R_2, respectively, is 1-3.5 %, assuming *NOE* values of 0.70 and above towards the theoretical limit (NOE^{max} (600 MHz) = 0.84, NOE^{max} (700 MHz) = 0.86 and NOE^{max} (900 MHz) = 0.89 for $S^2 = 1.0$, $\tau_{int} = 0$ ps, $\tau_c = 40$ ns and $R_1 = 0.3$ s^{-1} (700 MHz); see **Supplementary Fig. 5B**) as found among structured protein regions.

Thus, the above described analysis is only necessary, when highly accurate measurements are available, for example in case of small soluble proteins such as the GB3 domain[3], the error of the experimental relaxation rates is below 1% and the *NOE* is measured with comparably high accuracy. In case of detergent-solubilized membrane proteins, experimental errors are generally larger (see for example **Supplementary Table 5**). Thus, R_1 and R_2 can be directly used for further estimation of ρ and measurement of heteronuclear steady-state *NOE*s is not required.

In the following we will describe the basic equations, which correlate ^{15}N-R_1 and ^{15}N-R_2 relaxation rates with the orientation of the N-H vector. For backbone amides in ^{2}H,^{15}N-labelled proteins two mechanisms of spin relaxation

dominate, namely the chemical shift anisotropy (CSA) of the nitrogen and the dipole-dipole interaction (DD) between the nitrogen and the directly bonded amide proton. Thus, the longitudinal (R_1) and transverse (R_2) relaxation rates are represented as:

$$R_1 = R_{1,DD} + R_{1,CSA}$$

$$R_2 = R_{2,DD} + R_{2,CSA} + R_{ex}$$

The DD and CSA contributions can be expressed in terms of spectral density functions $J(\omega)$ as:

$$R_{1,DD} = \frac{1}{4} D^2 [J(\omega_H - \omega_N) + 3J(\omega_N) + 6J(\omega_H + \omega_N)]$$

$$R_{1,CSA} = \frac{1}{3} C^2 J(\omega_N)$$

$$R_{2,DD} = \frac{1}{8} D^2 [4J(0) + J(\omega_H - \omega_N) + 3J(\omega_N) + 6J(\omega_H + \omega_N) + 6J(\omega_H)]$$

$$R_{2,CSA} = \frac{1}{18} C^2 [4J(0) + 3J(\omega_N)]$$

with amplitudes

$$D = -\frac{\mu_0}{4\pi} \gamma_H \gamma_N \hbar \langle r_{NH}^{-3} \rangle$$

$$C = \gamma_N B_0 \Delta\sigma = \omega_N \Delta\sigma$$

$\langle r_{NH}^{-3} \rangle$ is the vibrationally averaged N–H bond distance, $\Delta\sigma$ is the anisotropy of the axially symmetric ^{15}N shielding tensor, B_0 is the external magnetic flux density and ω_N is the ^{15}N chemical shift.

R_{ex} represents the contribution to transverse relaxation rate R_2 from motions slower than the overall tumbling but fast enough to average chemical shifts (in the range from μs to ms). R_{ex} is proportional to the square of the chemical shift difference between exchanging states, $\Delta\delta$, and to ω_N. It can affect the apparent transverse relaxation rate only when $\Delta\delta \neq 0$[10]. An efficient way to check the potential presence of R_{ex} is therefore to plot the ratio of R_2 rates at two magnetic fields, $R_{2(B1)}/R_{2(B2)}$, as a function of residue number. Application to the relaxation rates of E73V hVDAC1 did not provide evidence for R_{ex} (**Fig. 1c**).

In the formulation of model-free approaches (*MFA*), spectral density functions describe the overall tumbling as isotropic with a correlation time τ_R. Because even small degrees of motional anisotropy influence relaxation rates, reorientational anisotropy has to be taken into account to avoid determination of false parameters of internal motion. To this end, model-free approach spectral density functions are combined with a spectral density function, which describes anisotropic molecular tumbling. The latter comprises five terms and is given as[11]:

$$J(\omega) = \sum_{i=1}^{5} A_i \frac{\tau_i}{1 + (\omega\tau_i)^2}$$

Correlation times τ_i are expressed by the principal components, D_k, of the rotational diffusion tensor according to:

$\tau_1 = (4D_1 + D_2 + D_3)^{-1}$,

$\tau_2 = (D_1 + 4D_2 + D_3)^{-1}$,

$\tau_3 = (D_1+D_2+4D_3)^{-1}$,

$\tau_4 = 6[D+(D^2-L^2)^{1/2}]^{-1}$,

and $\tau_5 = 6[D-(D^2-L^2)^{1/2}]^{-1}$

where $D = (D_1+D_2+D_3)/3$ and $L^2 = (D_1D_2+D_2D_3+D_3D_1)/3$. A useful way of representing the diffusion tensor is to calculate the overall rotational correlation time τ_C, the anisotropy A and the rhombicity η according to:

$$\tau_C = 1/[2(D_x+D_y+D_z)]$$

$$A = 2D_z/(D_x+D_y)$$

$$\eta = 1.5(D_y-D_x)/[D_z-0.5(D_y+D_x)]$$

with $D_x \le D_y \le D_z$.

Directional factors A_i describe the orientation of the relaxation vector in the molecule-fixed coordinate system in terms of the directional cosines l, m, n:

$A_1 = 3m^2n^2$,

$A_2 = 3l^2n^2$,

$A_3 = 3m^2l^2$,

$A_4 = (d-e)/2$,

$A_5 = (d+e)/2$

where

$d = 0.5[3(l^4+m^4+n^4)-1]$,

$e = [\delta_1(3l^4+6m^2n^2-1)+\delta_2(3m^4+6l^2n^2-1)+\delta_3(3n^4+6l^2m^2-1)]/6$,

and $\delta_i = (D_i-D)/(D^2-L^2)^{1/2}$.

A_i is normalized according to ($A_1 + A_2 + A_3 + A_4 + A_5 = 1$). The model-free spectral density function of an anisotropically tumbling molecule according to the formalism by Lipari and Szabo[12,13] can thus be rewritten as

$$J^{MFA}(\omega) = \frac{2}{5}\sum_{i=1}^{5} A_i \left[\frac{S^2\tau_i}{1+(\omega\tau_i)^2} + \frac{(1-S^2)\tau_{\mathrm{int},i}}{1+(\omega\tau_{int,i})^2} \right]$$

where $1/\tau_{\mathrm{int},i} = 1/\tau_i + 1/\tau_{\mathrm{int}}$.

The spectral density function for the extended model-free approach (*EMFA*) of an anisotropically tumbling molecule is then (assuming the existence of an additional slow motion, with the order parameter S_s^2 and its internal time $\tau_{int,s}$, being outside the extreme narrowing limit and slower than S_f^2 but faster than molecular tumbling):

$$J^{EMFA}(\omega) = \frac{2}{5}\sum_{i=1}^{5} A_i \left[\frac{S_f^2 S_s^2 \tau_i}{1+(\omega\tau_i)^2} + \frac{(1-S_{f,i}^2)\tau_{f,i}}{1+(\omega\tau_{f,i})^2} + \frac{S_f^2(1-S_{s,i}^2)\tau_{s,i}}{1+(\omega\tau_{s,i})^2} \right]$$

where $1/\tau_{k,i} = 1/\tau_i + 1/\tau_{k,i}$. The indices *f* and *s* correspond to fast and slow internal motions, respectively.

1074 experimental ^{15}N-R_1 and ^{15}N-R_2 rates of E73V hVDAC1 from the three static magnetic fields (proton frequency of 600, 700 and 900 MHz) were fitted according to four different models of internal motion: (i) a 2-parameter MFA with the order parameter S^2 and the time scale for internal motions τ_{int} (**Supplementary Fig. 6**), (ii) a 3-parameter MFA[12,13] including an additional R_{ex} term, (iii) a 4-parameter EMFA, and (iv) a 5-parameter EMFA[5,14], corresponding to the following models for local dynamics: (1) $\{S_f^2, \tau_{int,f}\}$; (2) $\{S_f^2, \tau_{int,f}, R_{ex}\}$; (3) $\{S_f^2, S_s^2, \tau_{int,s}, \tau_{int,f}\}$; (4) $\{S_f^2, S_s^2, \tau_{int,s}, \tau_{int,f}, R_{ex}\}$. To this end, a grid search was performed, searching for the minimum in the global target function χ, which is given by the weighted sum of squared residuals:

$$\chi = \sum_{i=1}^{N} \Gamma_i = \sum_{i=1}^{N} \sum_{j=1}^{M} [(P_{ij,\exp} - P_{ij,calc})^2 / \sigma_{ij}^2]$$

, where the sum is over M relaxation data for each of the N residues of E73 hVDAC1, and $P_{ij,calc}$ are the appropriate relaxation parameters calculated from the assumed model of internal motion. σ_{ij} are the standard deviations of the experimentally derived $P_{ij,exp}$. The global target function consists of the sum of partial target functions Γ_i , which characterize the fit quality for the i^{th} residue[15]. The final comparison of the global search results revealed that the simple 2-parameter MFA analysis fully reproduced the experimental inpu). Inclusion of an additional R_{ex} term (model 2) or additional slow motions (models 3 and 4)[14] did not provide statistically better fits (see below). The finding that the simplest 2-parameter model is sufficient for description of the ps-ns time scale dynamics of E73V hVDAC1 is in agreement with the magnetic field dependence of the ^{15}N-R_2 rates for each individual residue (**Fig. 17**). Notably, a large set of deposited relaxation parameters observed in globular proteins could be explained by the 2-parameter model[5].

Validation of the correctness of the relaxation model [(1) to (4)] for local motions with fully anisotropic global reorientation was done according to the F-test (Fisher-Snedecor test):

(1) {S_f^2 , $\tau_{int,f}$} vs. (2) {S_f^2 , $\tau_{int,f}$, R_{ex}}
n=1074
p_2-p_1 = 179
n-p_2 = 531

p_1=364; χ_1=5986.5
p_2=543; χ_2=4296.9

F_{obl}=1.17

$F_{tabl}(p_2\text{-}p_1, n\text{-}p_2; \alpha)$ thus F_{tabl}(179,531;0.01)=1.32
$F_{tabl}(p_2\text{-}p_1, n\text{-}p_2; \alpha)$ thus F_{tabl}(179,531;0.05)=1.22

(1) {S_f^2 , $\tau_{int,f}$} vs. (3) {S_f^2, S_s^2, $\tau_{int,s}$, $\tau_{int,f}$}
n=1074
p_1=348; χ_1=5986.5
p_2=726; χ_2=3631.4

p_2-p_1 = 362
n-p_2 = 348

F_{obl}=0.27

$F_{tabl}(p_2\text{-}p_1, n\text{-}p_2; \alpha)$ thus F_{tabl}(362,348;0.01)=1.28
$F_{tabl}(p_2\text{-}p_1, n\text{-}p_2; \alpha)$ thus F_{tabl}(362,348;0.05)=1.19

(1) {S_f^2 , $\tau_{int,f}$} vs. (4) {S_f^2, S_s^2, $\tau_{int,s}$, $\tau_{int,f}$, R_{ex}}
n=1074
p_1=364; χ_1=5986.5
p_2=901; χ_2=2862.8

p_2-p_1 = 537
n-p_2 = 173

F_{obl}=0.35

$F_{tabl}(p_2\text{-}p_1, n\text{-}p_2; \alpha)$ thus F_{tabl}(537,173;0.01)=1.35

$F_{tabl}(p_2\text{-}p_1,n\text{-}p_2;\alpha)$ thus $F_{tabl}(537,173;0.05)=1.23$

Relaxation data comprised 179 pairs of R_1, R_2 (n=1074) for 600 MHz, 700 MHz and 900 MHz. The p_1 and p_2 stand for the numbers of parameters used for each of four models. In all cases, $F_{obl} < F_{tabl}$ at two applied confidence levels, indicating that the simple two-parameter model for local motions is sufficient to describe the internal mobility of E73V hVDAC1.

The diffusion tensor parameters τ_C, A and η are used as input in Xplor-NIH[16–19] for structure refinement against the experimental ^{15}N-R_2/R_1 rates. We determined initial values for τ_C, A and η (**Supplementary Table 6**) through the model-free approach described above. Although this requires the coordinates of the protein, it is more reliable than a histogram approach, which is employed for residual dipolar couplings[17]. For the model-free analysis we used the X-ray structure of VDAC1 from mouse (mVDAC1) (PDB id: 3EMN)[20]. The resulting tensor parameters were used for refinement of the 3D structure of E73V hVDAC1 against 124 R_2/R_1 ratios in Xplor-NIH. The calculated ensemble of lowest energy conformations was well converged (**Fig. 1b**). Next, the lowest energy conformer was selected, the directional cosines were recalculated, and the experimental relaxation rates were again fitted with the 2-parameter MFA model (1) (local S_f^2 and $\tau_{int,f}$ parameters and 6 global parameters for fully anisotropic motion). This resulted in similar tensor parameters (**Supplementary Table 6**). The refined set of tensor parameters was again used for structure calculation and yielded virtually the same coordinates (in line with the results **in Supplementary Fig**. **7**). To further validate the possible impact of diffusion tensor parameters on the resulting ensemble of structures, we intentionally varied the anisotropy (A) and rhombicity (η) of the diffusion tensor and repeated the structure calculations (**Supplementary Fig. 7**). In agreement with previous studies for protein complexes[21], ±0.2 unit changes on anisotropy and 50-100% changes in rhombicity did not perturb the refined 3D structure. Indeed, τ_C was the most stable parameter with respect to the input directional cosines[5].

Structure calculations, experimental restraints and refinement

Structure determination of E73V hVDAC1 was performed in two steps using the Xplor-NIH software platform[16]. First, an initial set of conformations was obtained by folding the extended polypeptide chain against backbone torsion angles and side-chain χ_1 angles, which were estimated by TALOS-N[22] on the basis of the experimental chemical shifts, together with distance restraints from a 3D ^{15}N-edited HMQC-NOESY experiment, as well as hydrogen bond restraints that were verified by hydrogen/deuterium exchange experiments[1]. Details of the simulated annealing protocol, further on called *Protocol 1*, are listed in **Supplementary Table 1**. Subsequently the lowest energy structures were refined using the second protocol, named *Protocol 2* (**Supplementary Table 7**), which introduced the diffusion anisotropy energy terms[17]. We further tested different multidimensional torsion angle data base potentials, the `2D/3D QUARTS` potential[23–25], as well as the `torsionDB` potential[18]. Overall, the two potentials provided comparable results, in agreement with previous reports[18]. Because hVDAC1 is solubilized in micelles, we did not use global packing potentials, such as the radius of gyration term (R_{gyr})[16], which were optimized for soluble proteins. We also resigned from the hydrophobic contact potential (`residueAffPot`), which contains low-resolution information on hydrophobic contacts[26], because a β-barrel protein such as VDAC does not have a typical hydrophobic core.

According to experimental backbone chemical shifts (analyzed by the program PROMEGA[27]) and NOE cross-peak patterns, Pro^{136} of E73V hVDAC1 is in c*is*-conformation. All other proline residues are in *trans*-conformation.

SUPPLEMENTARY FIGURES

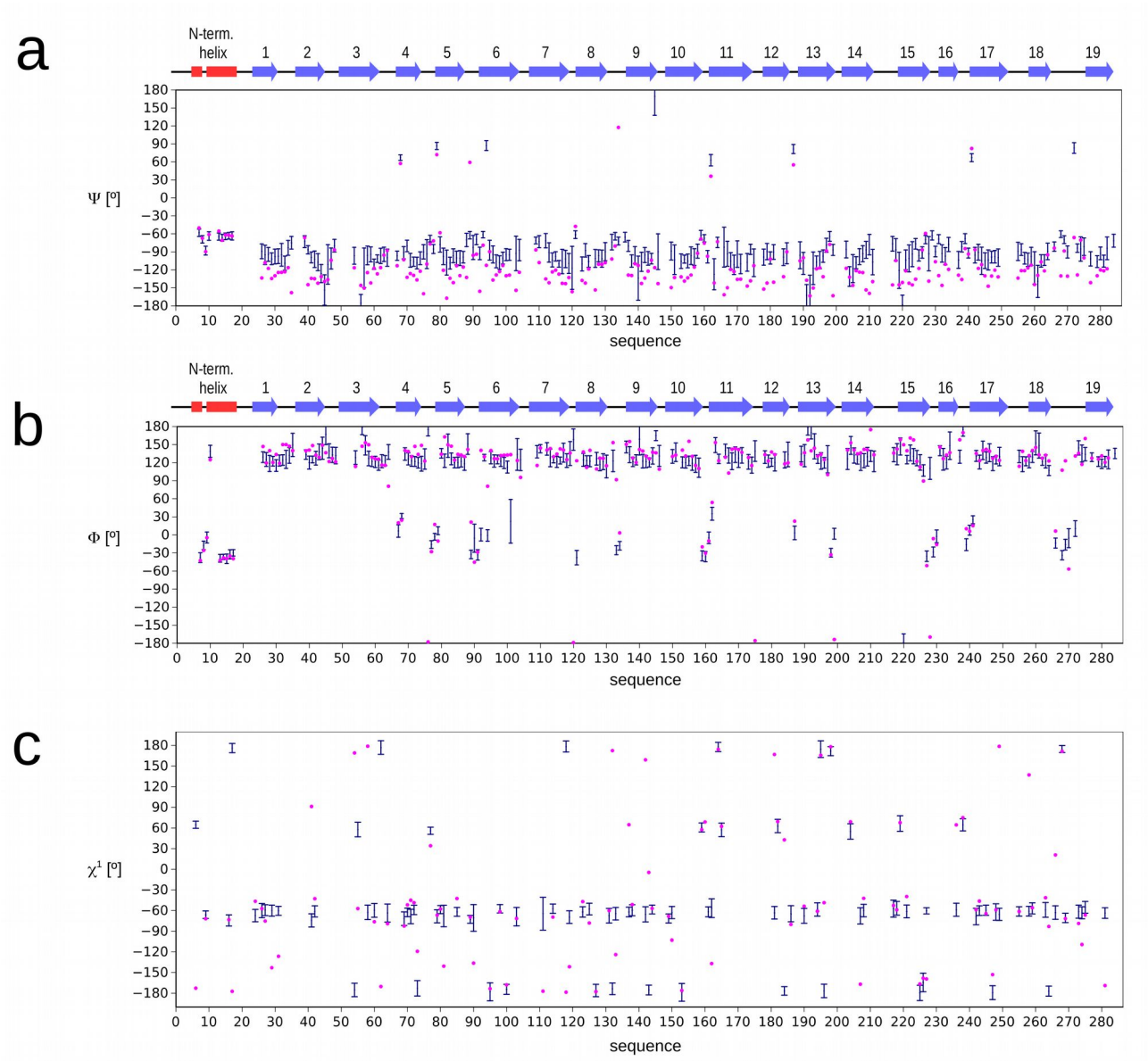

Suppl. Figure 1 | Torsion angle information from experimental chemical shifts. Backbone dihedral angles ψ (a), φ (b) and side-chain angles χ^1 on the basis of experimental backbone H^N, N, C^α, C' chemical shifts in E73V hVDAC1. Pink dots show the values observed in the crystal structure of mVDAC1 (PDB id: 3EMN) .

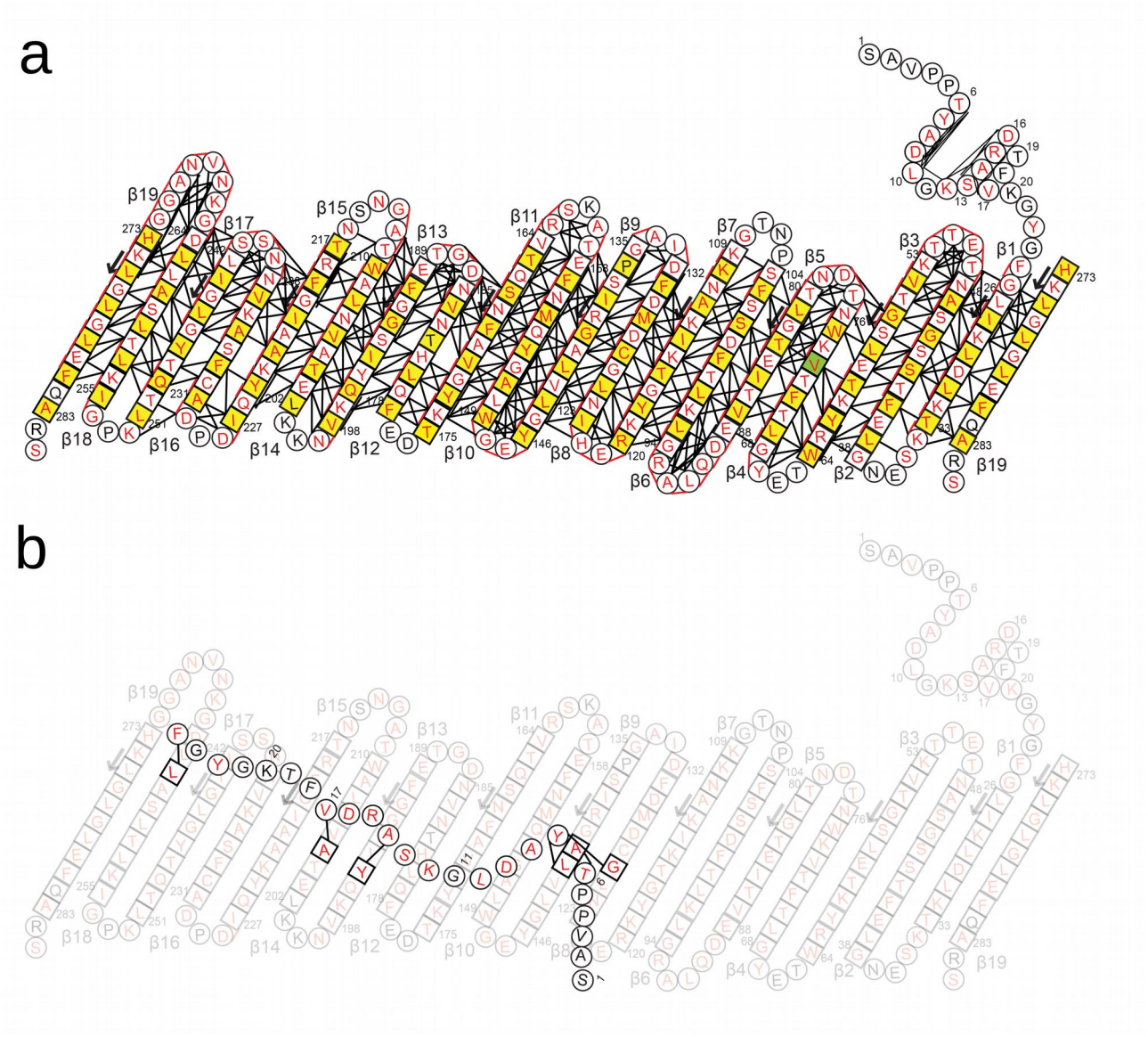

Suppl. Figure 2 | Assignment and network of NOEs in E73V hVDAC1. (**a**) Topology diagram of the secondary structure (β-strands as rectangles) of E73V hVDAC1, highlighting the H^N-H^N NOE network (black lines and red lined for the sequential contacts, respectively). Assigned residues are shown in red, unassigned residues in black. β-strands are labeled from 1 to 19 with β19 shown twice. Yellow rectangles mark residues for which the side-chain points towards the membrane. V73 is marked by a green rectangle. (**b**) H^N-H^N NOEs connecting the N-terminal helix to the barrel of E73V hVDAC1. NOEs were observed in a 3D ^{15}N-edited-HMQC-NOESY spectrum (mixing time 240 ms) recorded on U-^{2}H,^{15}N-labelled E73V hVDAC1 dissolved into 2% LDAO micelles.

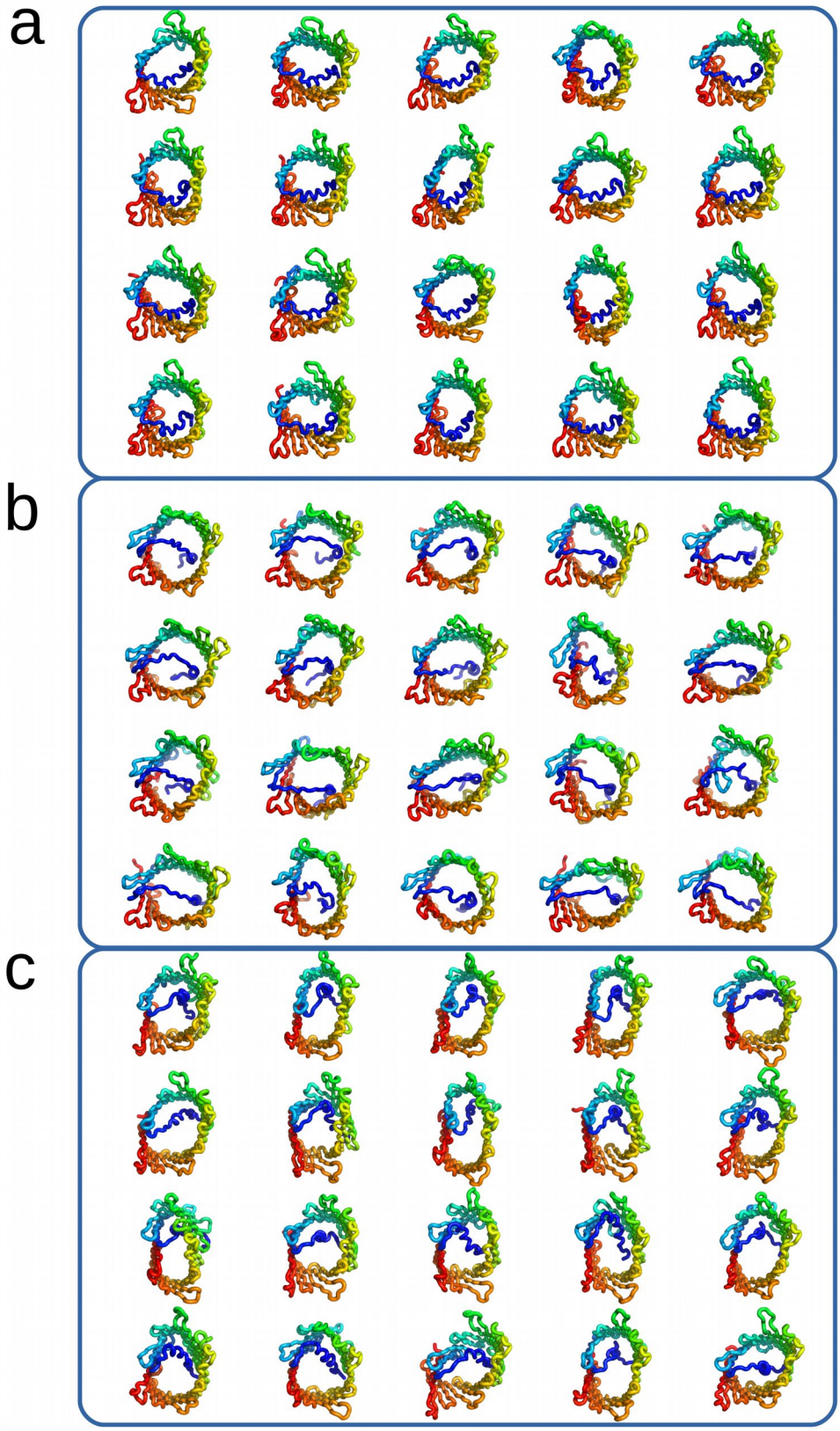

Suppl. Figure 3 | Different barrel shapes as found within the NOE-based 20 lowest-energy conformers of: (**a**) E73V hVDAC1 calculated exclusively from NOE-based and chemical shift-derived angular restraints according to *Protocol 1*, (**b**) hVDAC1 as reported in the 2K4T structural ensemble, (**c**) hVDAC1 calculated exclusively from the NOE and CS-derived angular data reported by Bayrhuber and co-workers[1] with *Protocol 1*. Structures are colored from the N- to the C-terminus from blue to red. NOE-based and chemical shift-derived restraints do not accurately define the shape of the hVDAC1 barrel.

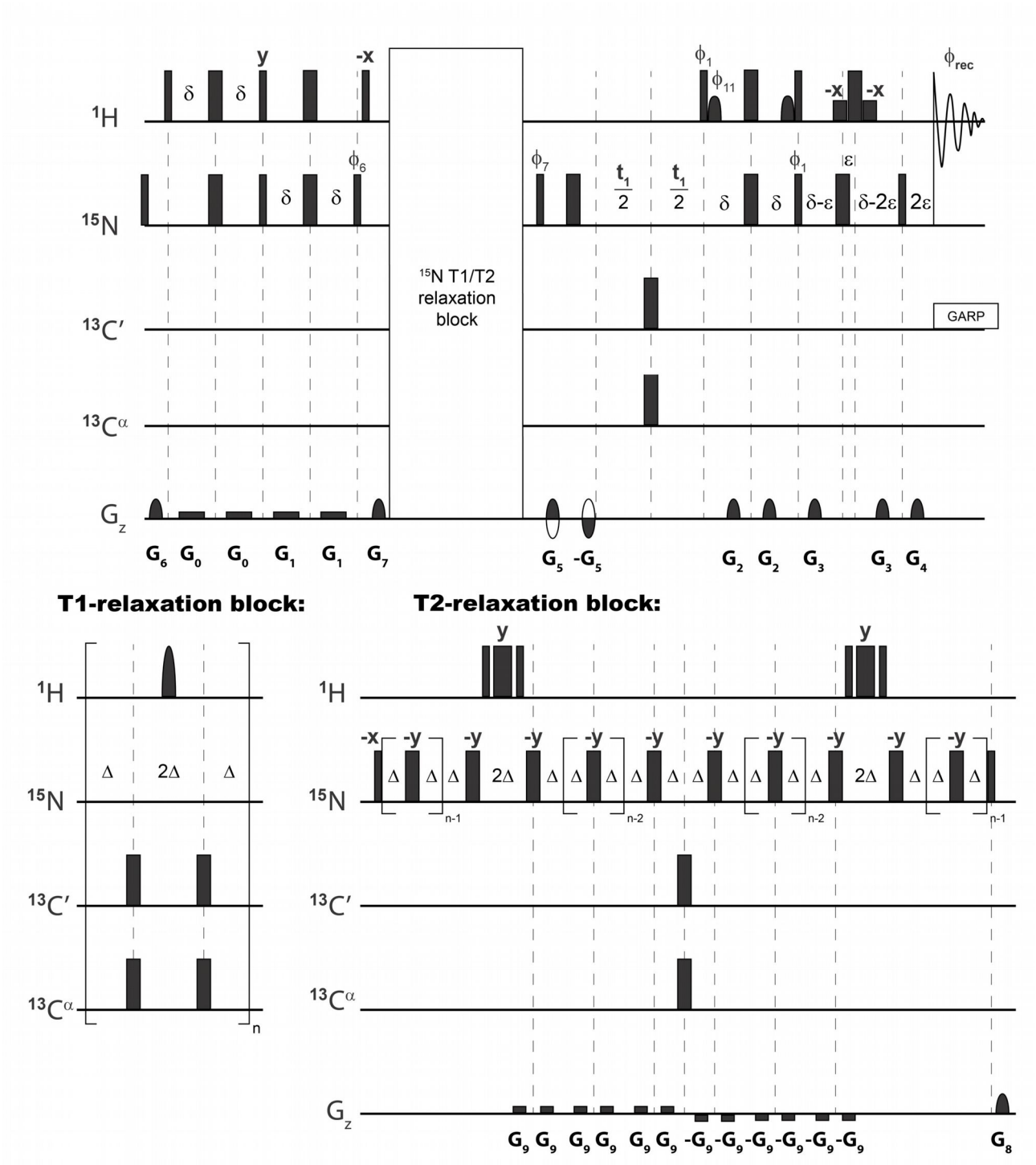

Suppl. Figure 4 | TROSY-based NMR pulse sequences for measurement of ^{15}N-R_1 and ^{15}N-R_2 pulse programs in high-molecular weight proteins. For each experiment the appropriate temperature compensation block (T-comp) was used (not shown in the scheme for clarity). For further details please see [3]. Δ in the T_2-relaxation block was set to 1.0 ms.

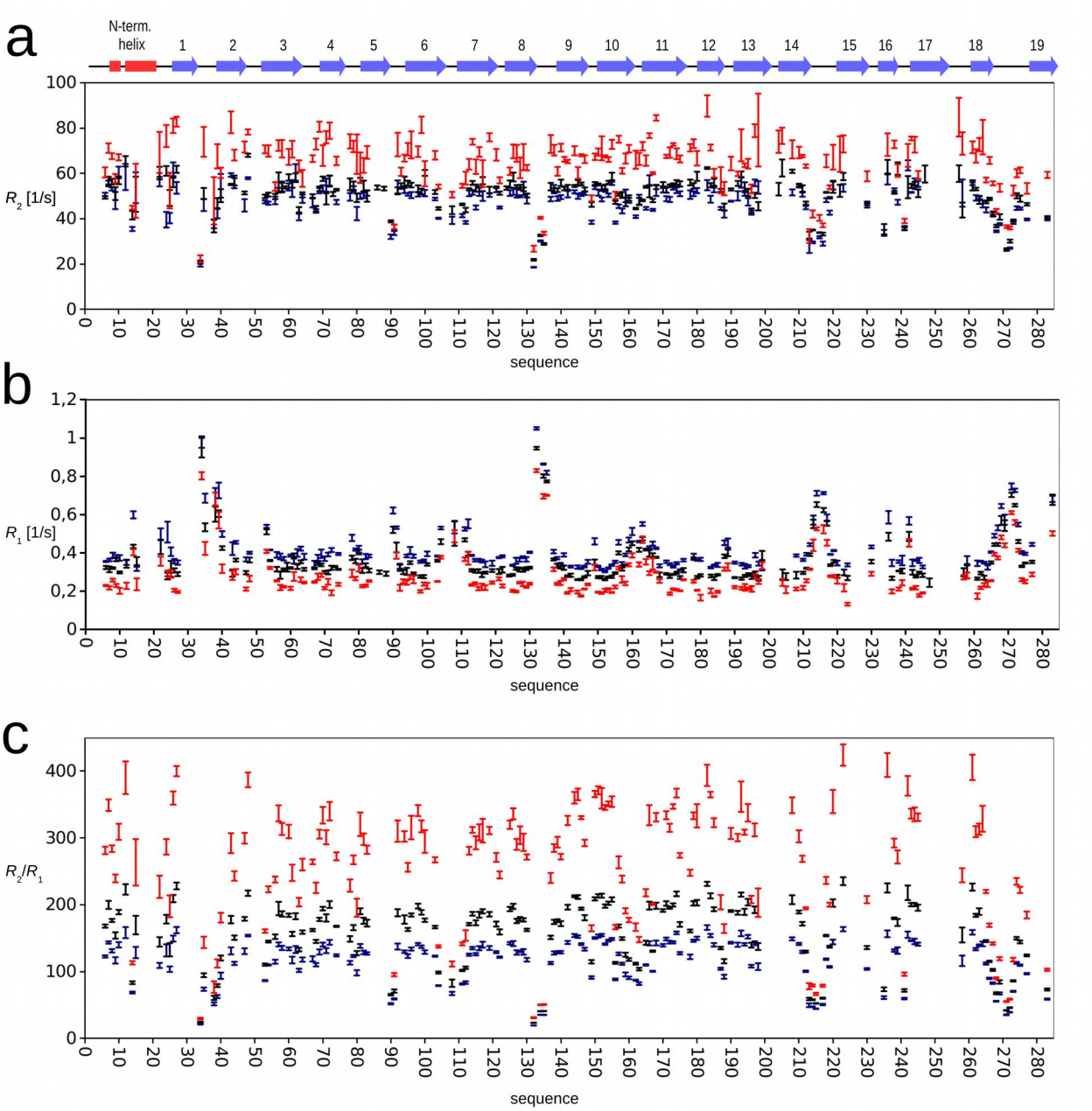

Suppl. Figure 5 | ^{15}N spin-relaxation rates observed in E73V hVDAC1 at three magnetic fields. (**a**) ^{15}N-R_2, (**b**) ^{15}N-R_1 and (**c**) R_2/R_1-ratios at 600 MHz (blue), 700 MHz (black) and 900 MHz (red) as function of the amino acid sequence. Experimental errors were determined as stated in the **Supplementart Information** section and their average values can be found in **Supplementary Table 5**. Experimental details on relaxation rate measurements are listed in **Supplementary Table 4.** Secondary motifs are marked with blue arrows (β-strands) and red rectangles (helix) on top.

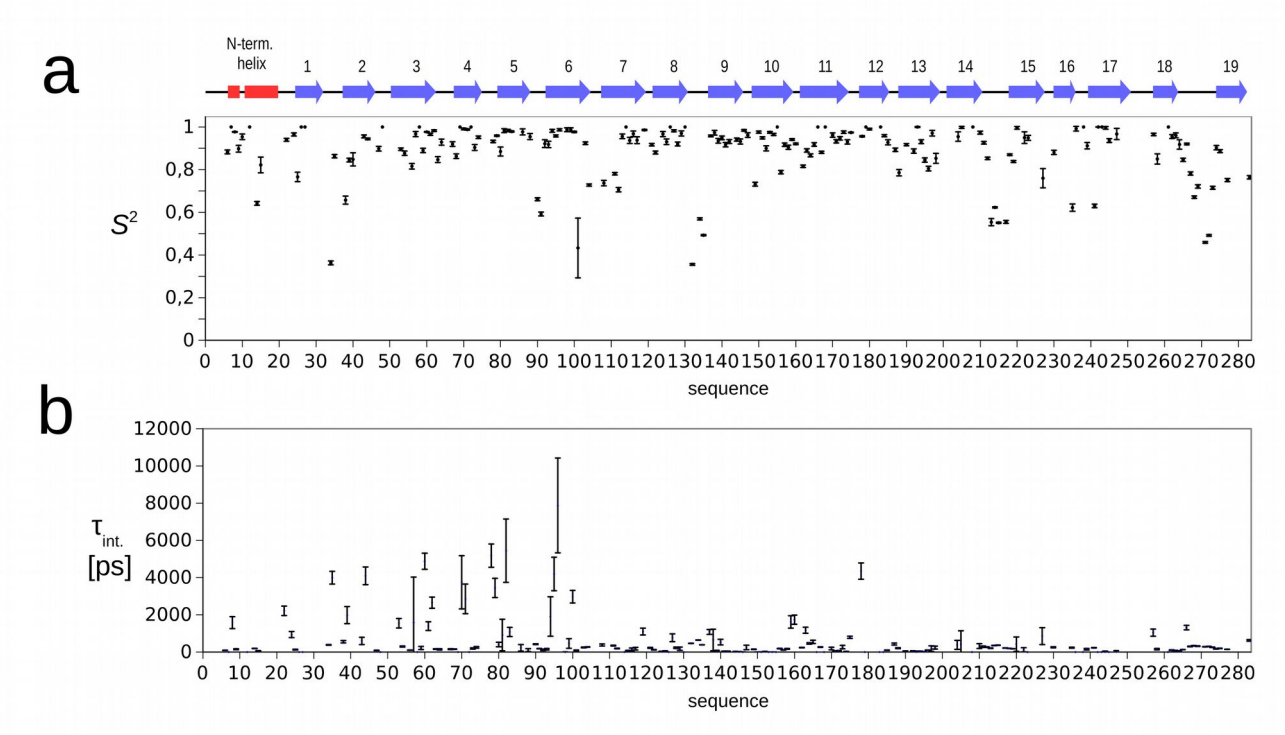

Suppl. Figure 6 | Model-free analysis of the ^{15}N relaxation data of E73V hVDAC1 (2-parameter MFA model with S_f^2 and $\tau_{int,f}$ and fully anisotropic reorientation). (**a**) Residue-specific S_f^2 order parameters. (**b**) Internal total correlation time ($\tau_{int,f}$) describing ps-ns time scale motions of individual residues. Errors were estimated by 200 Monte Carlo simulations and represent one s.d.. Secondary motifs are marked with blue arrows (β-strands) and red rectangles (helix) on top.

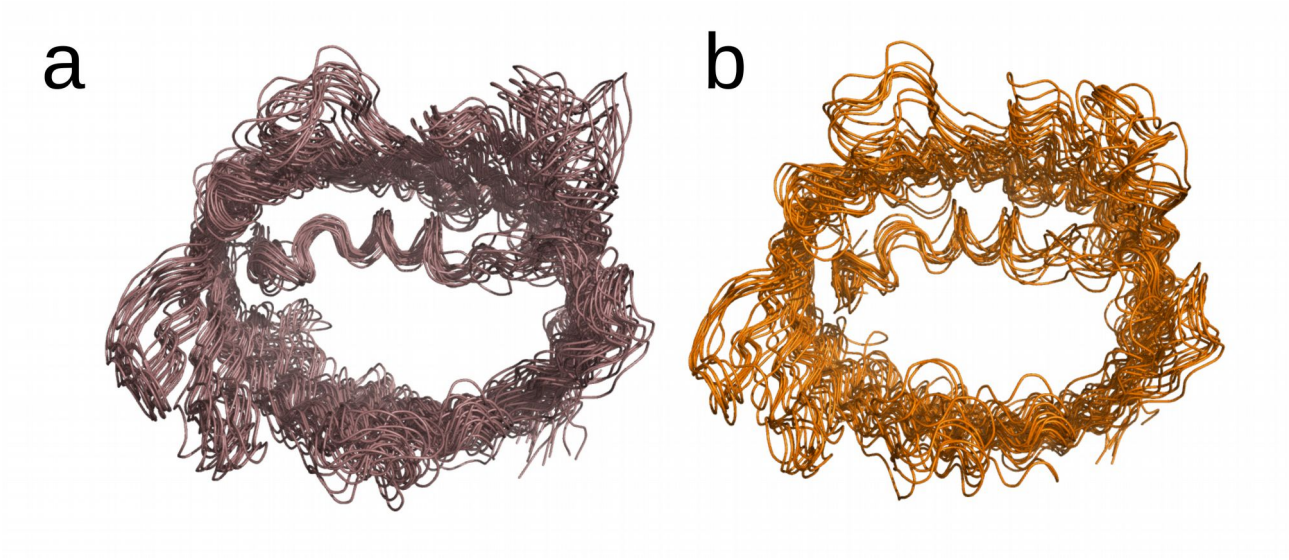

Suppl. Figure 7 | Influence of diffusion tensor parameters on the 3D structure. (**a**) Ensemble of 20 lowest-energy structures of E73V hVDAC1 after refinement against the experimental relaxation rates. (**b**) Superposition of the lowest-energy structures from 15 different runs, in which the tensor parameters and high-energy MD temperature step were varied. After refinement against the ^{15}N relaxation rates, the anisotropy A was 1.3, the rhombicity $\eta = 0.8$ and $\tau_c = 40$ ns. In the different calculations performed with *Protocol 2* the values of A, η, τ_c and the high-temperature dynamics values were varied as follows: 1.1 to 1.5 for A, 0.4 to 2.0 for η, 37 to 41 ns for τ_c and 500 to 3000K for the high-temperature dynamics step.

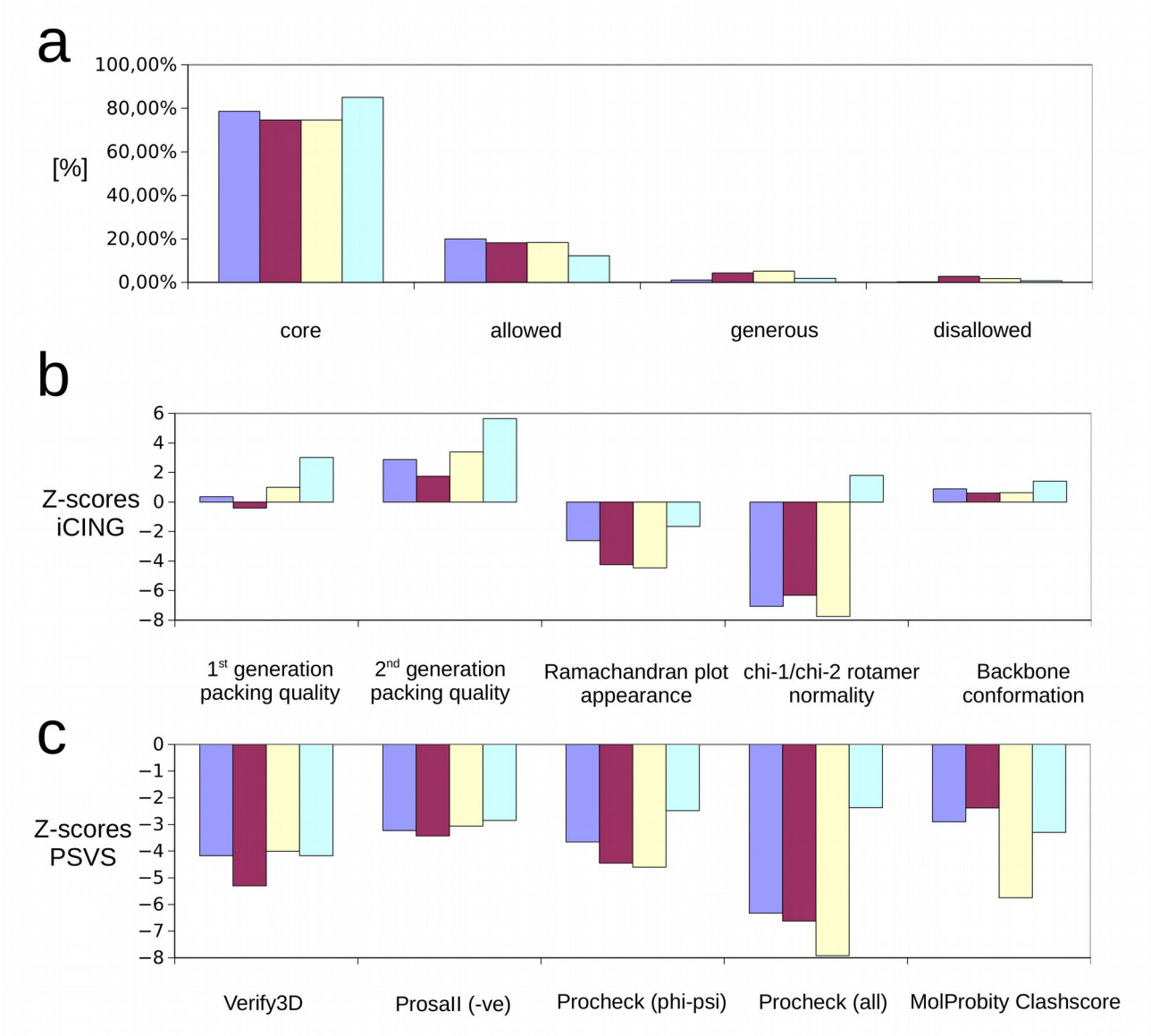

Suppl. Figure 8 | Quality Z-scores of hVDAC1 and E73V hVDAC1 before and after refinement against ^{15}N relaxation rates. (**a**) Ramachandran plot distribution. (**b**) iCING-derived Z-scores. (**c**) Z-scores derived from the Protein Structure Validation Software suite (PSVS). The following color coding is used: hVDAC1 as reported in [14] (blue; 1st column in Fig. 1b), hVDAC1 recalculated with *Protocol 1* on the basis of the NMR data reported in [13] (brown; 2nd column in Fig. 1b), E73V hVDAC1 derived from the new NMR data with Protocol 1 (cream; 3rd column in Fig. 1b) and refined against R_2/R_1-ratios with Protocol 2 (cyan; 4th column in Fig. 1b).

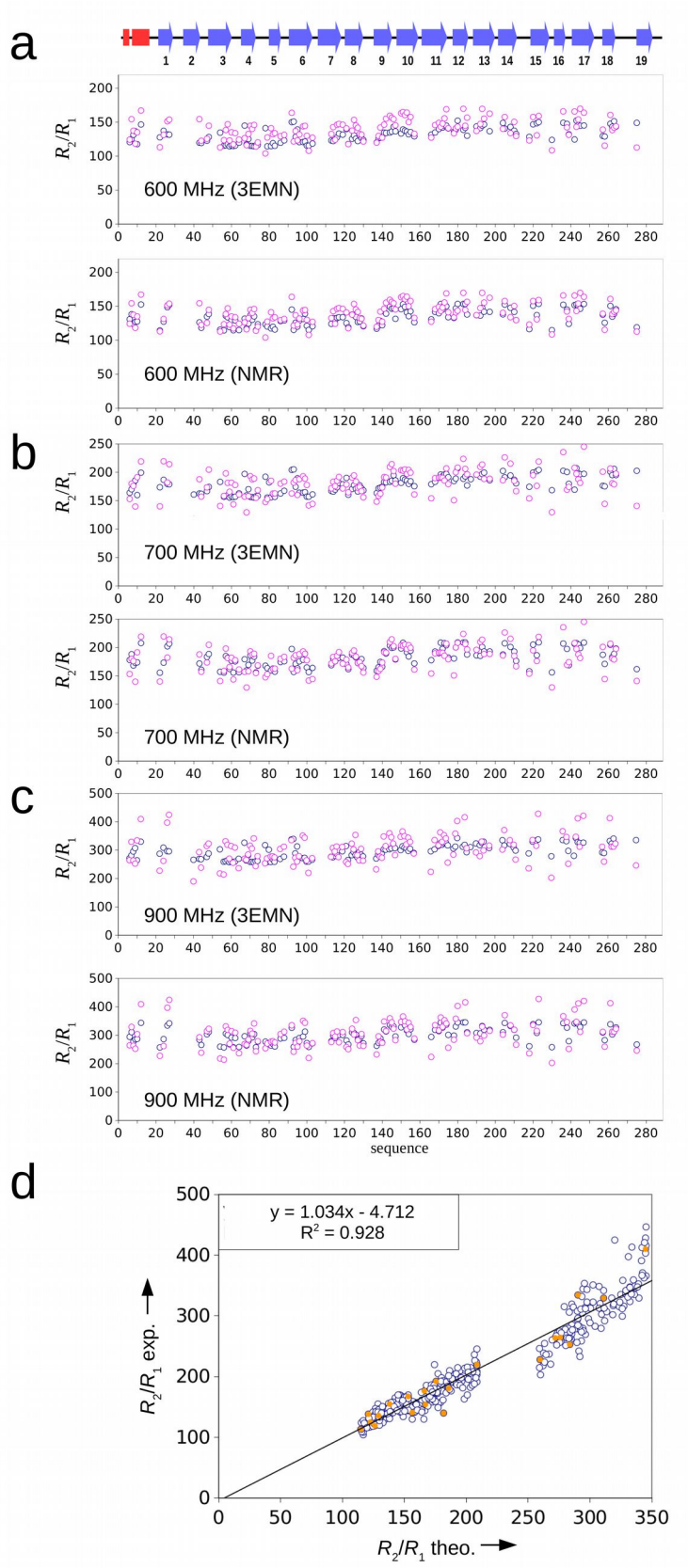

Suppl. Figure 9 | Comparison of experimental ^{15}N-R_2/R_1-ratios (pink) with values back-calculated from the 3D structure (blue) at 600 MHz (**a**), 700 MHz (**b**) and 900 MHz (**c**). In each panel upper and lower diagrams represent R_2/R_1-ratios that were back-calculated from the crystal structure of mVDAC1 (PDB id: 3EMN) and the lowest-energy structure of E73V hVDAC1 (Fig. 1b, 4th column), respectively. Error bars were omitted for clarity. The average error of the measured relaxation rates is listed in **Supplementary Table 5** and is comparable to the average r.m.s. between back-calculated and experimental R_2/R_1-ratios. (**d**) The circilar cross-validation of the 10% back-calculated and experimental R_2/R_1-ratios (from three magnetic fields) from 10 separate calculations for the lowest-energy structures refined adainst remaining 90% of R_2/R_1-ratios. Orange dots come from the N-terminal helix residues.

Supplementary Table 1. ***Protocol 1*** **used for structure calculation.** Xplor-NIH protocol for folding protein structures from an extended polypeptide chain against NMR-derived restraints.

- Step 1: Generation of extended strand conformation.
- Step 2: Torsion angle randomization.
- Step 3: High temperature torsion angle dynamics using NOE-derived distances, TALOS-N-derived torsion angles. Duration 800 ps.
- Step 4: Simulated annealing.
- Step 5: Final gradient minimization first in torsion angle space and then in Cartesian space.

Parameters for simulated annealing:
Starting temperature 3000 K
Final temperature 100 K
Temperature steps 12.5 K
Duration of simulations at every temperature: 0.5 ps or 8000 steps of molecular dynamics, whatever happens first.

The following potentials and force constants were used:

Potential term (unit of force constant)	**Restraints**	**Force constant**		
		High temperature dynamics	**Simulated annealing**	**Final minimization**
`NOEpot` (kcal/mol/Å^2)	square-well distance restraints from NOEs and hydrogen bonds	20	ramped from 20 to 100	100
`CDIH` (kcal/mol/rad^2)	square-well torsion angle restraints	500	500	500
`VDW` (kcal/mol/Å^4)	quartic atom-atom repulsion	0.01 Cα atoms	ramped from 0.01 to 4 for all atoms	4
`BOND` (kcal/mol/Å^2)	bond length	1000	1000	1000
`ANGLE` (kcal/mol/rad^2)	bond angle	200	ramped from 50 to 500	500
`IMPR` (kcal/mol/rad^2)	improper dihedral	50	ramped from 50 to 500	500
`RAMA*` (PMF)◊	multidimensional torsion angle data base potential, 2D and 3D QUARTS	0.02	ramped from 0.02 to 0.1	0.1
`torsionDB*` (PMF)	smoothed multidimensional torsion angle data base potential	0.02	ramped from 0.02 to 0.2	0.2
`HBDB` (PMF)	database for backbone H-bonds, used in *free mode*	E(x,y,z) = 0 E(θ''|r) = 0	E(x,y,z) = 0 E(θ''|r) = 0	E(x,y,z) = 0 E(θ''|r) = 0
`DANI` (kcal/mol)	Diffusion anisotropy refinement against R_2/R_1 ratios	0	0	0

* only one multidimensional torsion angle database potential was used at each structure determination and refinement cycle.
◊ PMF – potential of mean force.

Supplementary Table 2. NMR constraints and structural statistics for the ensemble of 20 lowest-energy structures of E73V hVDAC1 (Fig. 1b, third from left)

NOE-based distance constraints			
Total	656		
intra-residue [i = j]	0		
sequential [| i - j | = 1]	210		
medium range [1 < | i - j | < 5]	113		
long range [| i - j | ≥ 5]	333		
NOE constraints per restrained residue[b]	2.4		
Hydrogen bond constraints	256		
Dihedral-angle constraints:	447		
Total number of restricting constraints[b]	1359		
Total number of restricting constraints per restrained residue[b]	5.1		
Restricting long-range constraints per restrained residue[b]	2.1		
Total structures computed	200		
Number of structures used	20		
Residual constraint violations[a,c]			
Distance violations / structure			
0.1 - 0.2 Å	0.1		
> 0.2 Å	0		
RMS of distance violation / constraint	0.01 Å		
Maximum distance violation[d]	0.17 Å		
Dihedral angle violations / structure			
1 - 5 °	8		
> 5 °	0		
RMS of dihedral angle violation / constraint	0.28 °		
Maximum dihedral angle violation	4.00 °		
RMSD Values			
	all	ordered	
All backbone atoms	2.5 Å	2.1 Å	
All heavy atoms	3.0 Å	2.4 Å	
Structure Quality Factors - overall statistics			
	Mean score	SD	Z-score[g]
Procheck G-factor[e] (phi / psi only)	-1.25	N/A	-4.60
Procheck G-factor[e] (all dihedral angles)	-1.34	N/A	-7.92
Verify3D	0.22	0.0189	-3.85
ProsaII (-ve)	-0.10	0.0435	-3.10
MolProbity clashscore	43.00	4.6994	-5.85
Structure Z-scores (What-IF):			
1st generation packing quality	0.987 ± 0.767		
2nd generation packing quality	3.368 ± 1.633		
Ramachandran plot appearance	-4.457 ± 0.363		

χ^1/χ^2 rotamer normality	-7.759 ± 0.191
Backbone conformation	0.637 ± 0.178
Ramachandran Plot Summary from Procheck[f]	
Most favoured regions	74.7%
Additionally allowed regions	18.3%
Generously allowed regions	5.2%
Disallowed regions	1.8%

a) Analyzed for residues 1 to 285
b) There are 256 residues with conformationally restricting constraints.
c) Calculated for all constraints for the given residues, using sum over r^{-6}.
d) Largest constraint violation among all the reported structures.
e) Residues with sum of phi and psi order parameters > 1.8.
Ordered residue ranges:
f) Residues selected based on: all residues
Selected residue ranges: all
g) With respect to mean and standard deviation for a set of 252 X-ray structures < 500 residues, resolution <= 1.80 Å, R-factor <= 0.25 and R-free <= 0.28; a more positive or smaller negative value indicates a 'better' score.

Supplementary Table 3. NMR constraints and structural statistics for the ensemble of 20 lowest-energy structures of hVDAC1 calculated with *Protocol 1* on the basis of the NMR constraints reported by Bayrhuber *et al.* [1] (Fig. 1b, second from left)

NOE-based distance constraints	
Total	86
intra-residue [i = j]	0
sequential [| i - j | = 1]	13
medium range [1 < | i - j | < 5]	9
long range [| i - j | ≥ 5]	64
NOE constraints per restrained residue [b]	0.3
Hydrogen bond constraints	240
Dihedral-angle constraints	452
Total number of restricting constraints [b]	794
Total number of restricting constraints per restrained residue[b]	3.1
Restricting long-range constraints per restrained residue [b]	1.2
Total structures computed	200
Residual constraint violations [a,c]	
Distance violations	
0.1 - 0.2 Å	0.35
0.2 - 0.5 Å	0.95
> 0.5 Å	0
RMS of distance violation / constraint	0.00 Å
Maximum distance violation [d]	0.28 Å
Dihedral angle violations	
1 - 5 °	1.3
> 5 °	0
RMS of dihedral angle violation / constraint	0.13 °

Maximum dihedral angle violation	3.70 °		
RMSD Values			
	all	ordered	
All backbone atoms	3.8 Å	3.3 Å	
All heavy atoms	4.5 Å	3.6 Å	
Structure Quality Factors - overall statistics			
	Mean score	SD	Z-score[g]
Procheck G-factor[e] (phi / psi only)	-1.21	N/A	-4.45
Procheck G-factor[e] (all dihedral angles)	-1.12	N/A	-6.62
Verify3D	0.13	0.0177	-5.30
ProsaII (-ve)	-0.18	0.0408	-3.43
MolProbity clashscore	22.76	2.8711	-2.38
Structure Z-scores (What-IF)			
1st generation packing quality	-0.412 ± 0.931		
2nd generation packing quality	1.756 ± 1.528		
Ramachandran plot appearance	-4.244 ± 0.324		
χ^1/χ^2 rotamer normality	-6.317 ± 0.357		
Backbone conformation	0.603 ± 0.328		
Ramachandran Plot Summary from Procheck[f]			
Most favoured regions	74.7%		
Additionally allowed regions	18.2%		
Generously allowed regions	4.3%		
Disallowed regions	2.8%		

a) Analyzed for residues 1 to 285.
b) There are 256 residues with conformationally restricting constraints.
c) Calculated for all constraints for the given residues, using sum over r^{-6}.
d) Largest constraint violation among all the reported structures.
e) Residues with sum of phi and psi order parameters > 1.8.
Ordered residue ranges:
f) Residues selected based on: all residues
Selected residue ranges: all
g) With respect to mean and standard deviation for a set of 252 X-ray structures < 500 residues, resolution <= 1.80 Å, R-factor <= 0.25 and R-free <= 0.28; a more positive or smaller negative value indicates a 'better' score.

Supplementary Table 4. Acquisition parameters, which were used in the measurement of ^{15}N-R_1 and ^{15}N-R_2 relaxation rates in E73V hVDAC1.

T [K]	Exp	Field [T]	d1 [s]	Relaxation delays [ms]	^{1}H SW [Hz]	^{15}N SW [Hz]	^{1}H pts#	^{15}N pts#
310	R_1	14.1	5	0, 240, 560, 1000, 1520, 2400	8389.26	1945.42	1024	256
310	R_2	14.1	5	4, 8, 12, 16, 24, 32	8389.26	1945.42	1024	256
310	R_1	16.5	5	0, 320, 640, 960, 1520, 3040	11160.71	2272.73	1024	256
310	R_2	16.5	5	4, 8, 12, 16, 24, 32	11160.71	2272.73	1024	256
310	R_1	21.2	5	0, 320, 640, 1120, 1800, 3040	12626.26	2941.18	1024	256
310	R_2	21.2	5	4, 8, 12, 16, 20, 28	12626.26	2941.18	1024	256

these are Bruker FID data points.

Supplementary Table 5. Number of ^{15}N-R_1 and ^{15}N-R_2 relaxation rates, which were used for MFA analysis (left column) and structure calculation (right column), along with their average experimental errors.

Magnetic Field	**600 MHz**		**700 MHz**		**900 MHz**	
# of rates	**179**	**124**	**179**	**124**	**179**	**124**
ΔR_1	2.7 %	3.0 %	2.7 %	2.8 %	3.9 %	3.9 %
ΔR_2	2.7 %	2.9 %	3.1 %	3.0 %	4.4 %	4.2 %

Supplementary Table 6. Influence of starting coordinates on experimentally-driven and predicted diffusion tensor parameters. Reported tensor parameters without errors come from the best solution global search fit of the relaxation rates according to MFA (model 1) to the starting coordinates as stated in the first column. 'NMR R_2/R_1-refined (744)' indicates the lowest energy structure after the refinement against 744 relaxation rates according to *Protocol 2* (PDB id: 5JDP). Reported parameters and their errors are average values ± s.d. determined for the 10 lowest energy structures obtained by refinement according to *Protocol* 1 and *Protocol 2* with the later being labeled as 'NMR R_2/R_1-refined (1074)'.

Coordinates	**τ_C [ns]** [a]	**A** [b]	**η** [c]
mVDAC1 X-ray, 3EMN	39.2	1.24	0.83
hVDAC1 X-ray+NMR, 2JK4	39.7	1.33	0.87
NMR (*Protocol 1*; 1074)	40.1± 0.2	1.30 ± 0.06	0.87 ± 0.19
NMR R_2/R_1-refined (1074)	40.2 ± 0.1	1.32 ± 0.04	0.79 ± 0.18
NMR R_2/R_1-refined (744)	40.1	1.37	0.53

[a] total correlation time: $\tau_C = 1/[2(D_x+D_y+D_z)]$;
[b] anisotropy of the motion: $A = 2D_z/(D_x+D_y)$;
[c] rhombicity of the diffusion tensor: $\eta = 1.5(D_y-D_x)/[D_z-0.5(D_y+D_x)]$.

Below the table the inertia moment tensors (as 3×3 matrices) in the gravity center of different coordinates (specified by the PDB id) are listed together with the corresponding eigenvalues. Missing protons were added by PyMOL [28].

PDB id: 3EMN, anisotropy = 1.24,
$\begin{bmatrix} 8947\times10^3 & 568\times10^3 & 24\times10^3 \\ 568\times10^3 & 8258\times10^3 & -47\times10^3 \\ 24\times10^3 & -47\times10^3 & 10669\times10^3 \end{bmatrix}$, eigenvalues: 0.9268×10^7, 0.7937×10^7, 0.1067×10^8 [Å^2×Da];

PDB id: 2JK4, anisotropy = 1.21,
$\begin{bmatrix} 9211\times10^3 & 889\times10^3 & 415\times10^3 \\ 889\times10^3 & 10128\times10^3 & 237\times10^3 \\ 415\times10^3 & 237\times10^3 & 9338\times10^3 \end{bmatrix}$, eigenvalues: 0.8589×10^7, 0.1079×10^8, 0.9296×10^7 [Å^2×Da];

PDB id: 5JDP (the lowest energy structure), anisotropy = 1.27,
$\begin{bmatrix} 11460\times10^3 & -1272\times10^3 & -721\times10^3 \\ -1272\times10^3 & 10790\times10^3 & -1623\times10^3 \\ -721\times10^3 & -1623\times10^3 & 10038\times10^3 \end{bmatrix}$, eigenvalues: 0.1256×10^8, 0.8175×10^7, 0.1155×10^8 [Å^2×Da].

The same structures as above were selected for the prediction of the diffusion tensors by the HYDRONMR algorithm [28]. These calculations represent only the estimated values as if these proteins were soluble in solution. The HYDRONMR algorithm was designed and optimized for the analysis of globular proteins and takes into account solely the protein atoms (as the positions of the detergent molecules are not known) [29]. The settings were as follows: temperature set to 37°C, solvent viscosity 7.2×10^{-3} poise, radius of atomic elements set to 3.2 Å, minibeads generated

with σ(min) = 1.5 and σ(min) = 2.5, and remaining parameters as specified in the program by default.

HYDRONMR prediction for PDB id: 3EMN

eigenvector: $\begin{bmatrix} 0.8136 & 0.4146 & 0.4076 \\ -0.1421 & -0.5381 & 0.8308 \\ -0.5638 & 0.7339 & 0.3789 \end{bmatrix}$, eigenvalues: 1.020×10^{7}, 1.061×10^{7}, 1.163×10^{7} [s^{-1}];

HYDRONMR prediction for PDB id: 2JK4

eigenvector: $\begin{bmatrix} 0.6326 & 0.1888 & 0.7511 \\ 0.7276 & 0.1875 & -0.6599 \\ -0.2654 & 0.9639 & -0.0187 \end{bmatrix}$, eigenvalues: 9.464×10^{6}, 9.900×10^{6}, 1.055×10^{7} [s^{-1}];

HYDRONMR prediction for PDB id: 5JDP (the lowest energy structure)

eigenvector: $\begin{bmatrix} -0.2838 & 0.7810 & -0.5564 \\ -0.2224 & 0.5108 & 0.8304 \\ 0.9327 & 0.3594 & 0.0288 \end{bmatrix}$, eigenvalues: 9.603×10^{6}, 1.054×10^{7}, 1.140×10^{7} [s^{-1}].

The normalized scalar products beetween the HYDRONMR-predicted diffusion tensors from the raw protein coordinates are as follows:

	2JK4	mVDAC1 X-ray, 3EMN
5JPD	-0.58247	0.40055
2JK4	-	-0.44234

In addition normalized scalar products[30,31] between the fitted diffusion tensors to different coordinates (NMR R_2/R_1-refined – 5JPD or mVDAC1 X-ray of 3EMN) with the experimental relaxation data are listed.

	NMR R_2/R_1-refined (744)	mVDAC1 X-ray, 3EMN
NMR R_2/R_1-refined (1074)	0.99759	0.87770
NMR R_2/R_1-refined (744)	-	0.85253

The Euler angles[31] as determined from the best solution global search fit of the 1074 relaxation rates according to MFA (model 1) to the NMR R_2/R_1-refined structure (PDB id: 5JDP) are as follows:

ϑ = 19.8°, φ = -0.9°, ψ = -33.5°;

The angles define the spatial orientation of the diffusion tensor frame to the molecular frame of the protein which was set to the frame of the inertia tensor. As their values are not far from zero one can conclude that the detergent molecules (here LDAO) slightly influence the diffusive motion of the protein.

Supplementary Table 7. ***Protocol 2*** **used for structure calculation.** Xplor-NIH protocol and energy terms used for the refinement of NMR structures against ^{15}N-R_2/R_1 relaxation rates.

- Step 1: Reading of the coordinates obtained from *Protocol 1*
- Step 2: Powell minimization of geometry, fixing idealized geometry
- Step 3: High temperature torsion angle dynamics using NOE-derived distances, TALOS-N-derived torsion angles and ^{15}N-R_2/R_1 restraints. Duration 800 ps.
- Step 4: Simulated annealing.
- Step 5: Final gradient minimization first in torsion angle space and then in Cartesian space.

Parameters for simulated annealing:
Starting temperature 3000 K
Final temperature 100 K
Temperature steps 12.5 K
Duration of simulations at every temperature: 0.5 ps or 8000 steps of molecular dynamics, whatever happens first.

The following potentials and force constants were used:

Potential term (unit of force constant)	Restraints	Force constant		
		High temperature dynamics	Simulated annealing	Final minimization
NOEpot (kcal/mol/Å^2)	square-well distance restraints from NOEs and hydrogen bonds	20	ramped from 20 to 100	100
CDIH (kcal/mol/rad^2)	square-well torsion angle restraints	500	500	500
VDW (kcal/mol/Å^4)	quartic atom-atom repulsion	0.01 Cα atoms	ramped from 0.01 to 4 for all atoms	4
BOND (kcal/mol/Å^2)	bond length	1000	1000	1000
ANGLE (kcal/mol/rad^2)	bond angle	200	ramped from 50 to 500	500
IMPR (kcal/mol/rad^2)	improper dihedral	50	ramped from 50 to 500	500
RAMA (PMF◊)	multidimensional torsion angle data base potential, 2D and 3D QUARTS	0.25	ramped from 0.25 to 1	1
torsionDB (PMF)	smoothed multidimensional torsion angle data base potential	0.5	ramped from 0.5 to 2	2
HBDB (PMF)	database for backbone H-bonds, used in *free mode*	E(x,y,z) = 0.20 E(θ''|r) = 0.08	E(x,y,z) = 0.20 E(θ''|r) = 0.08	E(x,y,z) = 0.20 E(θ''|r) = 0.08
DANI (kcal/mol)	Diffusion anisotropy refinement against R_2/R_1 ratios	0.0001	ramped from 0.0001 to 0.25	0.25

◊ PMF – potential of mean force.

Supplementary Table 8. NMR constraints and structural statistics for the ensemble of 20 lowest-energy structures of E73V hVDAC1 obtained by refinement against 372 ^{15}N-R_2/R_1 restraints (Fig. 1B, fourth row). Structure quality factors were determined using PSVS 1.5 (http://psvs-1_5-dev.nesg.org) and iCING[32].

NOE-based distance constraints	
Total	656
intra-residue [i = j]	0
sequential [| i - j | = 1]	210
medium range [1 < | i - j | < 5]	113
long range [| i - j | ≥ 5]	333
NOE constraints per residue	2.5
Hydrogen bond constraints	256
Dihedral-angle constraints	452
Total number of restricting constraints [b]	1366
Total number of restricting constraints per restrained residue[b]	5.1
Restricting long-range constraints per restrained residue [b]	2.1
# of calculated structures	200

Residual constraint violations [a,c]			
Distance violations			
0.1 - 0.2 Å	1.9		
> 0.2 Å	0		
RMS of distance violations	0.01 Å		
Maximum distance violation [d]	0.20 Å		
Dihedral angle violations			
1 - 5 °	6.45		
> 5 °	0		
RMS of dihedral angle violation	0.26 °		
Maximum dihedral angle violation [d]	4.00 °		
RMSD Values			
	all	ordered	
All backbone atoms	1.1 Å	0.8 Å	
All heavy atoms	1.5 Å	1.2 Å	
Structure Quality Factors - overall statistics			
	Mean score	SD	Z-score[g]
Procheck G-factor[e] (phi / psi only)	-0.71	N/A	-2.48
Procheck G-factor[e] (all dihedral angles)	-0.40	N/A	-2.37
Verify3D	0.20	0.0161	-4.17
ProsaII (-ve)	-0.04	0.0309	-2.85
MolProbity clashscore	31.03	2.2978	-3.80
Structure Z-scores (What-IF; Vriend, 1990**):**			
1st generation packing quality	3.021 ± 0.849		
2nd generation packing quality	5.658 ± 1.668		
Ramachandran plot appearance	-1.661 ± 0.275		
χ^1/χ^2 rotamer normality	1.803 ± 0.350		
Backbone conformation	1.413 ± 0.209		
Ramachandran Plot Summary from Procheck [f]			
Most favoured regions	85.1 %		
Additionally allowed regions	12.3 %		
Generously allowed regions	1.9 %		
Disallowed regions	0.6 %		

a) Analyzed for residues 1 to 285.
b) There are 256 residues with conformationally restricting constraints.
c) Calculated for all constraints for the given residues, using sum over r^{-6}.
d) Largest constraint violation among all the reported structures.
e) Residues with sum of phi and psi order parameters > 1.8.
Ordered residue ranges:
f) Residues selected based on: all residues
Selected residue ranges: all
g) With respect to mean and standard deviation for a set of 252 X-ray structures < 500 residues, resolution <= 1.80 Å, R-factor <= 0.25 and R-free <= 0.28; a more positive or smaller negative value indicates a 'better' score.

References

[1] M. Bayrhuber, T. Meins, M. Habeck, S. Becker, K. Giller, S. Villinger, C. Vonrhein, C. Griesinger, M. Zweckstetter, K. Zeth, *Proc. Natl. Acad. Sci. U. S. A.* **2008**, *105*, 15370–5.

[2] S. Villinger, R. Briones, K. Giller, U. Zachariae, A. Lange, B. L. de Groot, C. Griesinger, S. Becker, M. Zweckstetter, *Proc. Natl. Acad. Sci. U. S. A.* **2010**, *107*, 22546–22551.

[3] N.-A. Lakomek, J. Ying, A. Bax, *J. Biomol. NMR* **2012**, *53*, 209–21.

[4] P. Damberg, J. Jarvet, A. Gräslund, *J. Am. Chem. Soc.* **2005**, *127*, 1995–2005.

[5] Ł. Jaremko, M. Jaremko, M. Nowakowski, A. Ejchart, *J. Phys. Chem. B* **2015**, *119*, 11978–11987.

[6] J. . MacDonald, *J. Magn. Reson.* **1980**, *38*, 381–384.

[7] D. Fushman, R. Varadan, M. Assfalg, O. Walker, *Prog. Nucl. Magn. Reson. Spectrosc.* **2004**, *44*, 189–214.

[8] R. Ghose, D. Fushman, D. Cowburn, *J. Magn. Reson.* **2001**, *149*, 204–17.

[9] D. Fushman, N. Tjandra, D. Cowburn, *J. Am. Chem. Soc.* **1998**, *120*, 10947–10952.

[10] J. W. Peng, G. Wagner, *Biochemistry* **1995**, *34*, 16733–16752.

[11] D. E. Woessner, *J. Chem. Phys.* **1962**, *37*, 647.

[12] G. Lipari, A. Szabo, R. M. Levy, *Nature* **1982**, *300*, 197–198.

[13] G. Lipari, A. Szabo, *J. Am. Chem. Soc.* **1982**, *104*, 4559–4570.

[14] G. M. Clore, A. Szabo, A. Bax, L. E. Kay, P. C. Driscoll, A. M. Gronenborn, *J. Am. Chem. Soc.* **1990**, *112*, 4989–4991.

[15] W. Press, S. Teukolsky, W. Vetterling, B. Flannery, E. Ziegel, W. Press, B. Flannery, S. Teukolsky, W. Vetterling, *Numerical Recipes: The Art of Scientific Computing*, **1987**.

[16] C. Schwieters, J. Kuszewski, G. M. Clore, *Prog. Nucl. Magn. Reson. Spectrosc.* **2006**, *48*, 47–62.

[17] N. Tjandra, D. S. Garrett, A. M. Gronenborn, A. Bax, G. M. Clore, *Nat. Struct. Biol.* **1997**, *4*, 443–449.

[18] G. a Bermejo, G. M. Clore, C. D. Schwieters, *Protein Sci.* **2012**, *21*, 1824–36.

[19] A. Grishaev, A. Bax, *J. Am. Chem. Soc.* **2004**, *126*, 7281–7292.

[20] R. Ujwal, D. Cascio, J.-P. Colletier, S. Faham, J. Zhang, L. Toro, P. Ping, J. Abramson, *Proc. Natl. Acad. Sci. U. S. A.* **2008**, *105*, 17742–7.

[21] A. D. J. van Dijk, R. Kaptein, R. Boelens, A. M. J. J. Bonvin, *J. Biomol. NMR* **2006**, *34*, 237–44.

[22] Y. Shen, A. Bax, *Methods Mol. Biol.* **2015**, *1260*, 17–32.

[23] J. Kuszewski, A. M. Gronenborn, G. M. Clore, *Protein Sci.* **1996**, *5*, 1067–1080.

[24] G. M. Clore, J. Kuszewski, *J. Am. Chem. Soc.* **2003**, *125*, 1518–1525.

[25] C. D. Schwieters, J. J. Kuszewski, G. Marius Clore, *Prog. Nucl. Magn. Reson. Spectrosc.* **2006**, *48*, 47–62.

[26] Y. Ryabov, J.-Y. Suh, A. Grishaev, G. M. Clore, C. D. Schwieters, *J. Am. Chem. Soc.* **2009**, *131*, 9522–31.

[27] Y. Shen, A. Bax, *J. Biomol. NMR* **2010**, *46*, 199–204.

[28] J. García de la Torre, M. L. Huertas, B. Carrasco, *J. Magn. Reson.* **2000**, *147*, 138–146.

[29] P. Bernadó, J. G. De la Torre, M. Pons, *J. Biomol. NMR* **2002**, *23*, 139–150.

[30] J. Sass, F. Cordier, A. Hoffmann, A. Cousin, J. G. Omichinski, H. Löwen, S. Grzesiek, *J Am Chem Soc* **1999**, *121*, 2047–2055.

[31] I. N. Bronshtein, K. A. Semendyayev, G. Musiol, H. M??hlig, *Handbook of Mathematics, Sixth Edition*, **2015**.

[32] J. F. Doreleijers, A. W. Sousa da Silva, E. Krieger, S. B. Nabuurs, C. A. E. M. Spronk, T. J. Stevens, W. F. Vranken, G. Vriend, G. W. Vuister, *J. Biomol. NMR* **2012**, *54*, 267–83.